Letter

Thermally induced local imbalance in repulsive binary Bose mixtures

G. Pascual,[1] G. Spada,[2] S. Pilati,[3,4] S. Giorgini,[2] and J. Boronat[1]

[1]*Departament de Física, Universitat Politècnica de Catalunya, Campus Nord B4-B5, E-08034 Barcelona, Spain*
[2]*Pitaevskii BEC Center, Dipartimento di Fisica and CNR-INO, Università di Trento, 38123 Povo, Trento, Italy*
[3]*School of Science and Technology, Physics Division, Università di Camerino, 62032 Camerino, Italy*
[4]*INFN-Sezione di Perugia, 06123 Perugia, Italy*

(Received 3 March 2023; accepted 26 July 2023; published 20 September 2023)

We study repulsive two-component Bose mixtures with equal populations and confined in a finite-size box through path-integral Monte Carlo simulations. For different values of the s-wave scattering length of the interspecies potential, we calculate the local population imbalance in a region of fixed volume inside the box at different temperatures. We find two different behaviors: For phase-separated states at $T = 0$, thermal effects induce a diffusion process which reduces the local imbalance, whereas for miscible states at $T = 0$, a maximum in the local population imbalance appears at a certain temperature, below the critical one. We show that this intriguing behavior is strongly related to the bunching effect associated with the Bose-Einstein statistics of the particles in the mixture and to an unexpected behavior of the cross pair distribution function.

DOI: 10.1103/PhysRevResearch.5.L032041

Introduction. The experimental realization of quantum Bose-Bose mixtures with dilute gases [1–5] has provided renewed interest in their theoretical study. Until this achievement, the only stable quantum mixture was the Fermi-Bose mixture composed by liquid ^{4}He and ^{3}He [6]. The Fermi nature of ^{3}He atoms was here crucial to understand the solubility observed in experiments [7], and in fact, it was proved theoretically that a fictitious Bose-Bose ^{3}He - ^{4}He mixture would always be unstable against phase separation [8]. With ultracold gases, the high tunability of interactions and the possibility of mixing species with different masses allow the exploration of full phase diagrams, in both the miscible and immiscible regimes. Recent work on these quantum mixtures has led to compelling findings such as the discovery of quantum droplets (for an attractive interspecies interaction) [9–11] or the occurrence of demixing phase transitions (for a repulsive interspecies interaction) [12–21].

In the case of repulsive interactions between all the particles of the mixture, a mean-field (MF) analysis at zero temperature shows that above the threshold $g_{12} = \sqrt{g_{11}g_{22}}$ (where g_{11} and g_{22} are the intraspecies coupling constants and g_{12} is the interspecies coupling constant) the two components of the mixture are phase separated and below that threshold, i.e., $g_{12} < \sqrt{g_{11}g_{22}}$, they are mixed [14]. A recent path-integral Monte Carlo (PIMC) study shows that the same condition on the interaction coupling constants holds also at finite temperature, distinguishing fully miscible from partially phase separated states [22]. In particular, this result rules out the possibility of a paramagnetic-to-ferromagnetic transition occurring with increasing temperature, which was predicted using beyond-mean-field perturbative theories [23–25]. Nonetheless, the behavior of Bose mixtures at finite temperature is a very interesting topic where effects from interactions and statistics combine producing an intriguing multicomponent superfluid phase.

The purpose of this Research Letter is to analyze the thermal behavior of a Bose-Bose mixture in a confined environment. To this end, we use the PIMC method, which is able to generate exact results for the thermodynamic properties of the system within controllable statistical errors. We use a box geometry like the one used in some recent experiments [26]. Our results for the local population imbalance show that its thermal behavior, below the Bose-Einstein transition temperature $T_{\rm BEC}$, is manifestly different for the states that at $T = 0$ are mixed or phase separated.

Model. We describe a system of two different bosons with total number of particles $N = N_1 + N_2$ in a cubic box of fixed volume V using the following microscopic Hamiltonian:

$$H = -\frac{\hbar^2}{2m_1}\sum_{i=1}^{N_1}\nabla_i^2 - \frac{\hbar^2}{2m_2}\sum_{i'=1}^{N_2}\nabla_{i'}^2 + \sum_{i<j}^{N_1} V(r_{ij}) + \sum_{i'<j'}^{N_2} V(r_{i'j'}) + \sum_{i,i'}^{N_1,N_2} V_{12}(r_{ii'}), \quad (1)$$

m_1 and m_2 being the masses of the two species and particle indexes i and i' indicating the coordinates of particles of species 1 and 2, respectively. We assume the same intraspecies potential for both components, $V(r)$, and study the influence on the properties of the mixture when the interspecies interaction $V_{12}(r)$ is changed. All the potentials are fully repulsive, and we use a continuous model of the form $V(r) = (\alpha/r)^{12}$ and $V_{12} = (\beta/r)^{12}$. The corresponding s-wave scattering lengths a

and a_{12} can be determined analytically from the parameters α and β, respectively [27,28]. Throughout this Research Letter we use a as the unit of length. Furthermore, our calculations are restricted to values of the gas parameter na^3 within the universal regime, in which the specific shape of the potential does not play any role [29]. To reduce the number of variables in our study, we consider all particles with the same mass $m = m_1 = m_2$ and the same number of particles for the two species $N_1 = N_2 = N/2$. The hard-wall conditions are imposed by rejecting any possible move of the particles outside the box. In the universal regime, the behavior of the mixture is only a function of the density, of the strengths $g = \frac{4\pi\hbar^2 a}{m}$ and $g_{12} = \frac{4\pi\hbar^2 a_{12}}{m}$, and of the temperature T. In particular, temperature is given in units of $T_{\rm BEC} = (2\pi\hbar^2/m) \cdot [n/(2\zeta(3/2))]^{2/3}$, where $n = N/V$ is the overall density in the box and $\zeta(x)$ is the Riemann zeta function.

Method. We have used the PIMC method to calculate in an exact way, within controllable statistical noise, the microscopic properties of the mixture at a given temperature. This method consists of dividing the thermal density matrix at some fixed T into multiple density matrices (called *beads*) at higher temperature, that can be well approximated [30]. In this Research Letter, we build the density matrix using the fourth-order Chin action [31], whose accuracy has been validated in applications to other quantum systems [32]. The simulations need to include the Bose symmetric statistics of the particles. To this end, we sample the permutation space using the worm algorithm [33]. To guarantee the distinguishability between particles of different species, we have introduced the sampling of a second worm, in the same way as it has been done in previous works [22,34].

The sampling in the PIMC method is conducted in the coordinate space; therefore properties that depend on position operators can be easily calculated. However, as simulations are performed in a finite-size box, some technical issues must be taken into account. In particular, the problem with studying local population imbalance in a cubic box is that the system is degenerate, i.e., there is no privileged direction along which particles exhibit population imbalance or, possibly, phase separation. Therefore, since the Monte Carlo simulation of the finite system samples all possible configurations and, as a result, all possible degeneracies, the average of the density profiles of the mixture masks any possible imbalance between particles of different species. To avoid this effect and to sum constructively any possible configuration, we calculate the center of mass for each component, and we define a one-dimensional density profile by integrating over particles along the axis joining the two centers of mass. In order to sample always the same slice of volume along the preferential axis, we only consider particles located inside a cylinder (see Fig. 1). Different shapes and different sizes of the cylinder have been tested obtaining, for all of them, compatible results.

The local population imbalance is calculated as follows:

$$\frac{\delta\tilde{N}}{\tilde{N}} = \frac{1}{2}\left(\int_{-L/(2\sqrt{2})}^{0} \frac{n_-(x)}{n_+(x)}dx - \int_{0}^{L/(2\sqrt{2})} \frac{n_-(x)}{n_+(x)}dx\right), \quad (2)$$

where $\tilde{N}$ is the total number of particles inside the cylinder, $n_+(x) = n_1(x) + n_2(x)$ and $n_-(x) = n_1(x) - n_2(x)$, and the sign of the axis joining the two centers of mass is chosen such that $n_2(x) > n_1(x)$ in the region $0 < x < L/(2\sqrt{2})$.

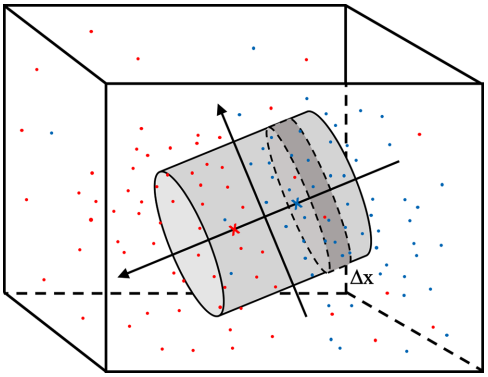

FIG. 1. Schematic view of the method used to estimate the density profiles. The two crosses, in red and in blue, represent the centers of mass of the two species, and the cylinder indicates the volume where the local population imbalance is calculated. The cylinder has the same diameter and length, $L/\sqrt{2}$, where L is the size of the cubic box.

Apart from ensuring the convergence of the results as a function of the number of *beads* used in the simulation, we analyze the imbalance $\delta\tilde{N}/\tilde{N}$ inside the cylinder with respect to the total number of particles in the box. In Fig. 2, we show the dependence of $\delta\tilde{N}/\tilde{N}$ on the total number N of particles in the box (at fixed overall density N/V). The results for the local imbalance decrease with increasing volume of the cylinder and are compatible with the expectation $\delta\tilde{N}/\tilde{N} = 0$ holding in the thermodynamic limit for a paramagnetic mixture.

Results. We fix the gas parameter to $na^3 = 10^{-4}$ for all the simulations. With this choice, the system is dilute enough to be in the universal regime [29], and at the same time, PIMC results converge faster than with smaller densities [34].

In Fig. 3, we show the density profiles along the axis of the cylinder of the two species (each curve of the same color represents the profile of components 1 and 2) at three different temperatures and for different values of g_{12}/g. For values below the phase-separation threshold $g_{12}/g = 1$ (top and middle plots), there is a constant trend: The peak of the density profiles becomes higher and more separated as the temperature is increased up to the maximum value $T = 0.7T_{\rm BEC}$. Moreover, for larger g_{12} values approaching the threshold this effect is enhanced. On the other hand, above $g_{12}/g = 1$ (bottom panel), that is, when the system is phase separated at $T = 0$, we see a clear suppression of the peak with increasing T consistent

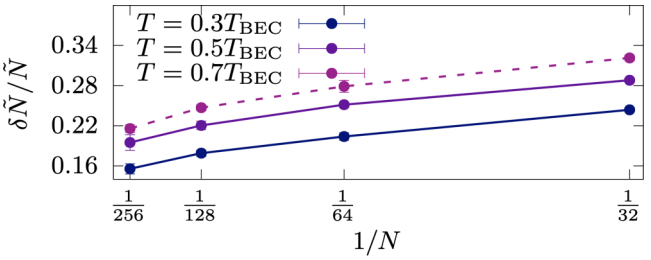

FIG. 2. Local population imbalance of the mixture with respect to the total number of particles at $g_{12}/g = 0.93$ and $na^3 = 10^{-4}$.

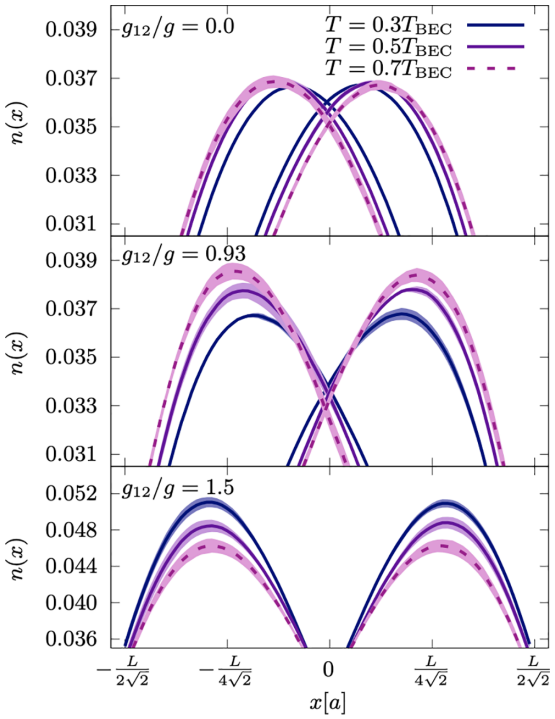

FIG. 3. Density profiles at different temperatures for different values of g_{12}/g. The shaded areas visualize the statistical error obtained by averaging over different configurations.

with a thermal behavior. In line with Fig. 3, Fig. 4 shows the corresponding behavior of the integrated local population imbalance $\delta\tilde{N}/\tilde{N}$ as a function of the temperature. For $g_{12}/g = 1.50$ the system is fully separated in the limit $T \to 0$, and by increasing the temperature, the local imbalance decreases monotonously, pointing to a tendency to mix. On the other hand, for values of $g_{12}/g \leqslant 1$, we see that the slope of $\delta\tilde{N}/\tilde{N}$ is positive at low temperature, showing a maximum imbalance at the characteristic temperature $T^\star \simeq 0.7T_{\rm BEC}$. By further increasing T, the local imbalance starts to decrease, and the local separation between species progressively vanishes. This effect is more evident when g_{12}/g approaches the threshold

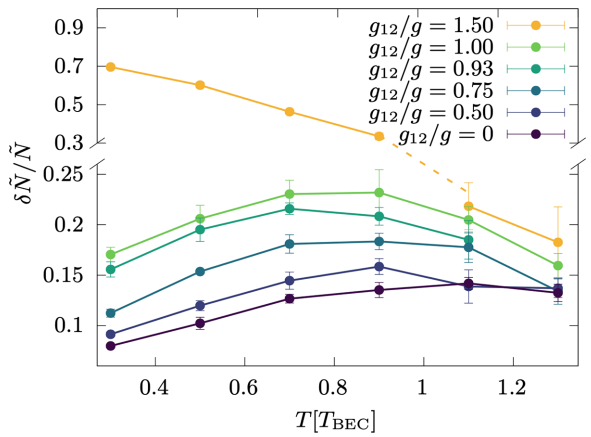

FIG. 4. Local population imbalance as a function of temperature for different values of g_{12}/g with $N = 256$. Note that the vertical axis is broken in order to show the different scale when $g_{12}/g > 1$.

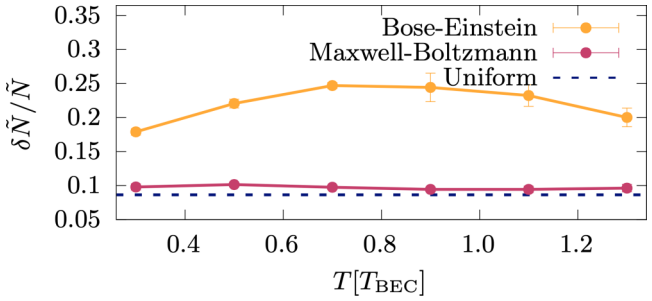

FIG. 5. Local population imbalance as a function of temperature for two different statistics at $g_{12}/g = 0.93$ with $N = 128$ obeying Bose-Einstein and Maxwell-Boltzmann statistics. The dashed line corresponds to a simulation with particles uniformly distributed in the box.

value. In the Appendix we show the effect on Fig. 4 of changing m_2/m_1 while keeping the same g_{12}/g.

It is interesting to explore further the origin of the peak in the local population imbalance for the case of mixed Bose gases at $T = 0$. To this end, we calculated $\delta\tilde{N}/\tilde{N}$ considering all the particles as distinguishable, that is, obeying the Maxwell-Boltzmann statistics. This is technically carried out by not sampling permutation cycles in the PIMC algorithm. As one can see in Fig. 5, distinguishable particles do not show any peak in the local imbalance giving evidence of a quantum effect led by the Bose-Einstein statistics of particles. Furthermore, we also compare these results with the ones from randomly generated configurations where particles are uniformly distributed in the box (dashed line in Fig. 5). We notice that, while both Maxwell-Boltzmann and uniformly distributed particles produce a finite value for $\delta\tilde{N}/\tilde{N}$ as a result of the procedure used to extract the local imbalance, this quantity does not show any peak as a function of temperature in sharp contrast with the case of Bose statistics. Furthermore, the result in Fig. 4 corresponding to the case $g_{12} = 0$, of independent components, displays a similar trend with T. Thus a possible explanation for part of the effect points toward the bunching mechanism, which enhances short-range correlations between identical Bose particles. However, interspecies interactions within the miscible regime $g_{12} < g$ also play an important role by producing the maximum in the local imbalance.

In order to better understand the role of statistics and interactions, we calculate the pair distribution function between particles of the same species $[\mathcal{G}_{11}(r)]$ and between particles of different species $[\mathcal{G}_{12}(r)]$. These observables are properly defined in homogeneous systems, where they only depend on the relative distance r between particles and approach unity at large separations. For this reason we compute them in the bulk using periodic boundary conditions, for a system with the same total density n and temperature T.

Figure 6 shows the temperature dependence of $\mathcal{G}_{11}(r)$ and $\mathcal{G}_{12}(r)$ (left and right panels, respectively) in the region of distances on the order of the mean interparticle separation. The bunching effect due to Bose statistics is active between particles of the same species and is responsible for the peak in $\mathcal{G}_{11}$. We notice that the hard-core repulsion used in our model reduces to zero the probability of finding two particles at very

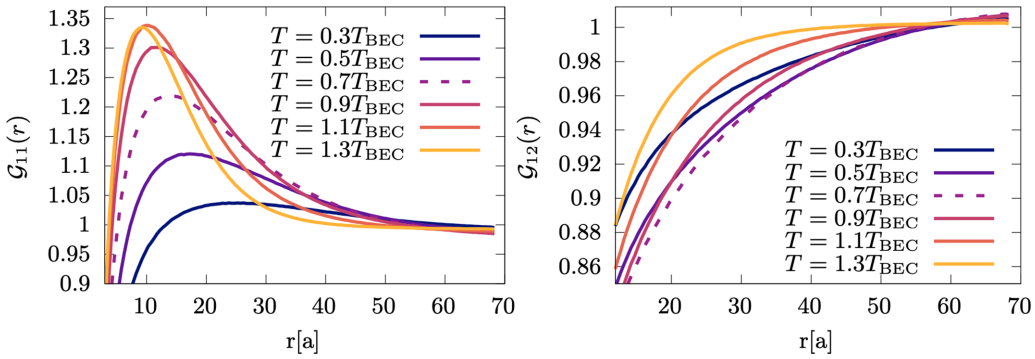

FIG. 6. Pair distribution functions between particles of the same species (left) and of different species (right) at $g_{12}/g = 0.9$ with $N = 256$ particles. These results have been computed in the same way as in Ref. [22] with periodic boundary conditions. In the left panel we can see the bunching effect between particles of the same species due to the Bose statistics. In the right panel we see an increase in the repulsion between particles of different species until $T_{\rm BEC} = 0.7$, where we start seeing the opposite trend.

short distances ($r[a] < 10$) at any temperature, whereas the peak in $\mathcal{G}_{11}$ increases with T and becomes narrower. This is a consequence of bunching correlations within the distance λ_T reaching a maximum at $T_{\rm BEC}$, while the thermal wavelength $\lambda_T = \sqrt{2\pi\hbar^2/mk_BT}$ shrinks with temperature. In contrast, $\mathcal{G}_{12}$ shows a different behavior: Up to $T \sim 0.7T_{\rm BEC}$ the curve is shifted to the right showing an increase in the repulsion between particles of different species, while for larger temperatures the curve is shifted to the left. The combined effect of bunching and the interaction effect visible in $\mathcal{G}_{12}$ is probably responsible for the behavior seen in Fig. 4. It is worth mentioning that an indication of a maximum in the repulsive interspecies correlations at $T \sim 0.7T_{\rm BEC}$ is also provided by the minimum of the interspecies contact parameter at approximately the same temperature [22].

Conclusions and discussion. We study binary Bose mixtures using the PIMC method in a confined box geometry for different values of g_{12}/g. We define a local observable probing the structure of the mixture, in particular its local magnetization, for a finite number of particles. Different behaviors are found for this local population imbalance as temperature is increased: For independent mixtures, $g_{12} = 0$, the imbalance increases steadily for all temperatures below $T_{\rm BEC}$, and vice versa, for interacting mixtures in the immiscible regime with $g_{12} > g$ we find a monotonous decrease. In the miscible regime, $0 < g_{12} < g$, we find instead a nonmonotonous behavior, featuring a broad maximum around $T \sim 0.7T_{\rm BEC}$. At approximately the same temperature we also observe a maximum of the interspecies repulsion measured by the pair distribution function.

We interpret these findings as a result of thermal effects, statistics, and interactions. The case $g_{12} > g$ is dominated by interactions. At zero temperature, the mixture is fully phase separated, and any finite temperature gives rise to a chemical potential gradient which makes the ground state unstable against particles of one species diffusing inside the region occupied by the other species [35]. The result is a tendency toward mixing which becomes stronger for increasing temperatures. The case $g_{12} = 0$ follows instead from the bunching effect which involves mainly thermally induced statistical correlations. As is well known, identical Bose particles tend to group together within a distance on the order of λ_T, and such bunching correlations are enhanced if the condensate is thermally depleted and $T_{\rm BEC}$ is approached from below. The most interesting regime, $0 < g_{12} < g$, features a more subtle interplay between interaction and statistical thermal effects. At any temperature T, the equilibrium state is a paramagnetic mixture exhibiting zero polarization in the thermodynamic limit [22]. However, a local partial imbalance between the two components can be the most probable state of a finite-size system. For such a system, bunching tends to increase the imbalance with T, similarly to the $g_{12} = 0$ case. Repulsive interactions between the two components make the effect of bunching more pronounced up to the characteristic temperature $T \sim 0.7T_{\rm BEC}$, where interspecies repulsion reaches a maximum. For higher temperatures the extra bunching provided by g_{12} is reduced, and the behavior of the local imbalance resembles again the case of independent components.

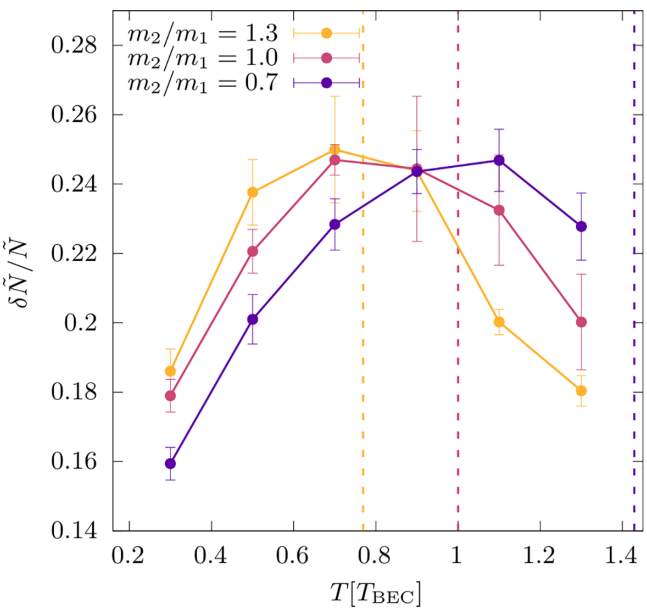

FIG. 7. Local population imbalance as a function of temperature for different mass ratios. The vertical dashed lines correspond to the $T_{\rm BEC,2}$.

Previous works found a similar local partial separation in other quantum systems, such as a gas in a disk-shaped harmonic trap [36] or a gas with dipolar interactions [37], but neither of them reported a maximum in the local imbalance at a certain temperature below T_{BEC}. Furthermore, although the bunching effect is a well-known feature in Bose gas, the nonmonotonous behavior of the interspecies pair distribution function $\mathcal{G}_{12}(r)$ in a binary mixture is something that can lead to interesting phenomena. The present experimental technology for producing box potentials [26] and the use of absorption imaging in a quasi-two-dimensional system [38] could be an ideal setup for exploring these deep quantum phenomena.

Acknowledgments. This work has been supported by the Spanish Ministry of Universities under FPU Grant No. FPU20/00013 and the Spanish Ministry of Economics, Industry and Competitiveness under Grant No. PID2020-113565GB-C21. G.S., S.G., and S.P. acknowledge the Italian Ministry of University and Research under the PRIN2017 project CEnTraL (Protocol No. 20172H2SC4). S.P. also acknowledges support from PNRR MUR Project No. PE0000023-NQSTI and from PRACE, for awarding access to the Fenix Infrastructure resources at Cineca, which are partially funded from the European Union Horizon 2020 research and innovation program through the ICEI project under Grant Agreement No. 800858. S.G. acknowledges also cofunding by European Union NextGenerationEU. Views and opinions expressed are however those of the authors only and do not necessarily reflect those of the European Union or the European Research Council. Neither the European Union nor the granting authority can be held responsible for them.

APPENDIX: IMBALANCED MASS RATIOS

When we increase the mass of the particles of the second species, we reduce its critical temperature ($T_{\mathrm{BEC},2} = \frac{m_1}{m_2} T_{\mathrm{BEC}}$), and as a result the maximum in the polarization is shifted to lower temperatures (see Fig. 7). This can be understood as, when one of the two critical temperatures is changed, the thermal window where the two species remain in a BEC phase, and thus feel the bunching effect, is also modified (shortened and lengthened in the yellow and purple cases, respectively, in Fig. 7).

[1] C. J. Myatt, E. A. Burt, R. W. Ghrist, E. A. Cornell, and C. E. Wieman, Production of Two Overlapping Bose-Einstein Condensates by Sympathetic Cooling, Phys. Rev. Lett. **78**, 586 (1997).

[2] D. M. Stamper-Kurn, M. R. Andrews, A. P. Chikkatur, S. Inouye, H.-J. Miesner, J. Stenger, and W. Ketterle, Optical Confinement of a Bose-Einstein Condensate, Phys. Rev. Lett. **80**, 2027 (1998).

[3] J. Stenger, S. Inouye, D. M. Stamper-Kurn, H.-J. Miesner, A. P. Chikkatur, and W. Ketterle, Spin domains in ground-state Bose–Einstein condensates, Nature (London) **396**, 345 (1998).

[4] G. Modugno, M. Modugno, F. Riboli, G. Roati, and M. Inguscio, Two Atomic Species Superfluid, Phys. Rev. Lett. **89**, 190404 (2002).

[5] G. Thalhammer, G. Barontini, L. De Sarlo, J. Catani, F. Minardi, and M. Inguscio, Double Species Bose-Einstein Condensate with Tunable Interspecies Interactions, Phys. Rev. Lett. **100**, 210402 (2008).

[6] C. Ebner and D. O. Edwards, The low temperature thermodynamic properties of superfluid solutions of ^{3}He in ^{4}He, Phys. Rep. **2**, 77 (1970).

[7] A. Fabrocini and A. Polls, Variational study of ^{3}He - ^{4}He mixture, Phys. Rev. B **25**, 4533 (1982).

[8] T. Chakraborty, Variational theory of binary boson mixture at $T = 0$ K, Phys. Rev. B **25**, 3177 (1982).

[9] D. S. Petrov, Quantum Mechanical Stabilization of a Collapsing Bose-Bose Mixture, Phys. Rev. Lett. **115**, 155302 (2015).

[10] C. R. Cabrera, L. Tanzi, J. Sanz, B. Naylor, P. Thomas, P. Cheiney, and L. Tarruell, Quantum liquid droplets in a mixture of Bose-Einstein condensates, Science **359**, 301 (2018).

[11] G. Semeghini, G. Ferioli, L. Masi, C. Mazzinghi, L. Wolswijk, F. Minardi, M. Modugno, G. Modugno, M. Inguscio, and M. Fattori, Self-Bound Quantum Droplets of Atomic Mixtures in Free Space, Phys. Rev. Lett. **120**, 235301 (2018).

[12] B. D. Esry, C. H. Greene, J. P. Burke, Jr., and J. L. Bohn, Hartree-Fock Theory for Double Condensates, Phys. Rev. Lett. **78**, 3594 (1997).

[13] H. Pu and N. P. Bigelow, Properties of Two-Species Bose Condensates, Phys. Rev. Lett. **80**, 1130 (1998).

[14] P. Ao and S. T. Chui, Binary Bose-Einstein condensate mixtures in weakly and strongly segregated phases, Phys. Rev. A **58**, 4836 (1998).

[15] E. Timmermans, Phase Separation of Bose-Einstein Condensates, Phys. Rev. Lett. **81**, 5718 (1998).

[16] M. Trippenbach, K. Góral, K. Rzazewski, B. Malomed, and Y. B. Band, Structure of binary Bose-Einstein condensates, J. Phys. B: At., Mol. Opt. Phys. **33**, 4017 (2000).

[17] C. J. Pethick and H. Smith, *Bose-Einstein Condensation in Dilute Gases* (Cambridge University Press, Cambridge, 2001).

[18] D. J. McCarron, H. W. Cho, D. L. Jenkin, M. P. Köppinger, and S. L. Cornish, Dual-species Bose-Einstein condensate of ^{87}Rb and ^{133}Cs, Phys. Rev. A **84**, 011603(R) (2011).

[19] L. Wacker, N. B. Jørgensen, D. Birkmose, R. Horchani, W. Ertmer, C. Klempt, N. Winter, J. Sherson, and J. J. Arlt, Tunable dual-species Bose-Einstein condensates of ^{39}K and ^{87}Rb, Phys. Rev. A **92**, 053602 (2015).

[20] F. Wang, X. Li, D. Xiong, and D. Wang, A double species ^{23}Na and ^{87}Rb Bose–Einstein condensate with tunable miscibility via an interspecies Feshbach resonance, J. Phys. B: At., Mol. Opt. Phys. **49**, 015302 (2015).

[21] K. L. Lee, N. B. Jørgensen, L. J. Wacker, M. G. Skou, K. T. Skalmstang, J. J. Arlt, and N. P. Proukakis, Time-of-flight expansion of binary Bose–Einstein condensates at finite temperature, New J. Phys. **20**, 053004 (2018).

[22] G. Spada, L. Parisi, G. Pascual, N. G. Parker, T. P. Billam, S. Pilati, J. Boronat, and S. Giorgini, Phase separation in binary Bose mixtures at finite temperature, arXiv:2211.09574.

[23] M. Ota, S. Giorgini, and S. Stringari, Magnetic Phase Transition in a Mixture of Two Interacting Superfluid Bose Gases at Finite Temperature, Phys. Rev. Lett. **123**, 075301 (2019).

[24] M. Ota and S. Giorgini, Thermodynamics of dilute Bose gases: Beyond mean-field theory for binary mixtures of Bose-Einstein condensates, Phys. Rev. A **102**, 063303 (2020).

[25] A. Rakhimov, T. Abdurakhmonov, Z. Narzikulov, and V. I. Yukalov, Self-consistent theory of a homogeneous binary Bose mixture with strong repulsive interspecies interaction, Phys. Rev. A **106**, 033301 (2022).

[26] N. Navon, R. Smith, and Z. Hadzibabic, Quantum gases in optical boxes, Nat. Phys. **17**, 1334 (2021).

[27] S. Pilati, K. Sakkos, J. Boronat, J. Casulleras, and S. Giorgini, Equation of state of an interacting Bose gas at finite temperature: A path-integral Monte Carlo study, Phys. Rev. A **74**, 043621 (2006).

[28] L. D. Landau and E. M. Lifshitz, *Quantum Mechanics (Nonrelativistic Theory)* (Pergamon, Oxford, 1977), p. 550.

[29] S. Giorgini, J. Boronat, and J. Casulleras, Ground state of a homogeneous Bose gas: A diffusion Monte Carlo calculation, Phys. Rev. A **60**, 5129 (1999).

[30] D. M. Ceperley, Path integrals in the theory of condensed helium, Rev. Mod. Phys. **67**, 279 (1995).

[31] S. A. Chin and C. R. Chen, Gradient symplectic algorithms for solving the Schrödinger equation with time-dependent potentials, J. Chem. Phys. **117**, 1409 (2002).

[32] K. Sakkos, J. Casulleras, and J. Boronat, High order Chin actions in path integral Monte Carlo, J. Chem. Phys. **130**, 204109 (2009).

[33] M. Boninsegni, N. V. Prokof'ev, and B. V. Svistunov, Worm algorithm and diagrammatic Monte Carlo: A new approach to continuous-space path integral Monte Carlo simulations, Phys. Rev. E **74**, 036701 (2006).

[34] G. Pascual and J. Boronat, Quasiparticle Nature of the Bose Polaron at Finite Temperature, Phys. Rev. Lett. **127**, 205301 (2021).

[35] A. Roy and D. Angom, Thermal suppression of phase separation in condensate mixtures, Phys. Rev. A **92**, 011601(R) (2015).

[36] H. Ma and T. Pang, Condensate-profile asymmetry of a boson mixture in a disk-shaped harmonic trap, Phys. Rev. A **70**, 063606 (2004).

[37] P. Jain and M. Boninsegni, Quantum demixing in binary mixtures of dipolar bosons, Phys. Rev. A **83**, 023602 (2011).

[38] C.-L. Hung, X. Zhang, L.-C. Ha, S.-K. Tung, N. Gemelke, and C. Chin, Extracting density–density correlations from *in situ* images of atomic quantum gases, New J. Phys. **13**, 075019 (2011).